

Phase-Space Evolution of Dark Matter Halos

S. Peirani^{1,2} and J. A. de Freitas Pacheco³

¹ Institut d'Astrophysique de Paris, 98 bis Bd Arago, 75014 Paris, France - UMR 7095 CNRS - Université Pierre et Marie Curie
e-mail: peirani@iap.fr

² Department of Physics, University of Oxford, Denys Wilkinson Building, Keble Road, Oxford OX1 3RH, UK

³ Observatoire de la Côte d'Azur - Laboratoire Cassiopée - UMR 6202 - BP 4229 - 063 04 - Nice Cedex 4 - France
e-mail: pacheco@oca.eu

Received ..., ...; accepted ..., ...

ABSTRACT

Context. In a Universe dominated by dark matter, halos are continuously accreting mass (violently or not) and such mechanism affects their dynamical state.

Aims. The evolution of dark matter halos in phase-space, and using the phase-space density indicator $Q = \rho/\sigma^3$ as a tracer, is discussed.

Methods. We have performed cosmological N -body simulations from which we have carried a detailed study of the evolution of ~ 35 dark halos in the interval $0 \leq z \leq 10$.

Results. The follow up of individual halos indicates two distinct evolutionary phases. First, an early and fast decrease of Q associated to virialization after the gravitational collapse takes place. The nice agreement between simulated data and theoretical expectations based on the spherical collapse model support such a conjecture. The late and long period where a slow decrease of the phase-space density occurs is related to accretion and merger episodes. The study of some merger events in the phase-space (radial velocity versus radial distance) reveals the formation of structures quite similar to caustics generated in secondary infall models of halo formation. After mixing in phase-space, halos in quasi-equilibrium have flat-topped velocity distributions (negative kurtosis) with respect to Gaussians. The effect is more noticeable for captured satellites and/or substructures than for the host halo.

Key words. dark matter – Galaxies: halos – Galaxies: interactions – Methods: N-body Simulations

1. Introduction

In the cold dark matter paradigm, galaxies are formed when baryonic gas falls into the gravitational potential well of cold dark matter (CDM) halos. These halos evolve by accreting mass either by quasi continuous processes or by merger events, when their masses vary sudden and significantly. Mass accretion is also an important mechanism by which halos acquire angular momentum after turnaround, since during the collapse phase tidal torques become inefficient (Peirani et al. 2004). Moreover, Wechsler et al. (2002) found an important correlation between accretion and the halo concentration. Halos in a state of high accretion have central densities related to the background density while those with low infall rates have approximately constant central densities.

After a merger episode, the resulting halo is not in equilibrium. Rapid variations in the gravitational potential contribute to the relaxation of the resulting system through a well known mechanism dubbed “violent relaxation” (Lynden-Bell, 1967). This process, after a few dynamical time scales ($t_{\text{dyn}} \sim 1/\sqrt{G\bar{\rho}}$), produces a smooth mass-independent distribution function (DF) as a result of the gravitational scattering of particles. Violent relaxation leads to a more mixed system (Tremaine et al. 1986), reducing the value of the coarse-grained DF. Mixing effects were also considered by Dehnen (2005), who has investigated the behavior of the *excess-mass function* $D(f)$ defined in a phase-space volume where the coarse-grained distribution function is greater than a given value f . For central density profiles represented by a power law ($\rho \propto r^{-\gamma}$), Dehnen (2005) found that $D \propto f^{-2(3-\gamma)/(6-\gamma)}$, suggesting that steeper cusps are less

mixed that shallower ones. As a corollary, if halos having different power law density profiles merge, the resulting halo cannot have a cusp steeper than those of the progenitors. A similar approach was adopted by Arad et al. (2004), who defined instead the function $v(f)$ such as $v(f)df$ be the phase-space volume occupied by phase-space elements where the density lies in the range $f, f + df$. They have found from cosmological simulations that $v(f)$ is quite well described by a power law, e.g., $v(f) \propto f^{-2.5 \pm 0.05}$, over three to five decades in f . According to them, such a power law behavior reflects the halo substructure, consequence of the hierarchical clustering and not the result of violent relaxation.

Investigations on the resulting equilibrium state after a merger episode, based on numerical simulations, use in general a more simple estimator for the coarse-grained DF defined as $Q = \rho/\sigma^3$, where ρ and σ are respectively the density and the cube of the 1-D velocity dispersion of dark matter particles inside a considered volume. High resolution simulations of galaxy-size CDM halos indicate an increase of Q towards the center (Taylor & Navarro, 2001) and similar results were obtained by Boylan-Kolchin & Ma (2004), Rasia et al. (2004), Ascasibar et al. (2004), Dehnen & McLaughlin (2005), Hoffman et al. (2007), Ascasibar & Gottlöber (2008), Vass et al (2008a, 2008b), who have also obtained a power-law variation, e.g., $Q \propto r^{-\beta}$ for cluster-size halos, with β quite close to the value found by Taylor & Navarro, namely, $\beta \approx 1.87$. Moreover, similar trends have been found by Knollmann, Knebe & Hoffman (2008) considering different cosmogonies although they found that the slope β depends on the concentration parameter of dark matter halos.

No adequate explanation presently exists for such a power-law profile which describes the phase-space density profile in dark halos. However, Austin et al. (2005) used semi analytic extended secondary infall models to show that such a behavior is a robust feature of virialized halos, which have attained equilibrium via violent relaxation and not the result of hierarchical merging, a conclusion in contradiction with that by Arad et al. (2004).

Analyses of the phase-space density in the core of dwarf spheroidal galaxies, rotating dwarfs, low surface brightness galaxies and clusters suggest another scaling law, e.g., $Q \propto \sigma^{-n}$, with $n \sim 3-4$ (Dalcanton & Hogan, 2001). This scaling can be understood if the merging halos were initially close to equilibrium and if the fusion process preserves approximately the physical density as each layer is homologously added to form the new system (Dalcanton & Hogan, 2001). A scaling relation close to $Q \propto \sigma^{-3}$ was obtained from cosmological simulations by Davé et al. (2001) for collisionless as well as for self-interacting dark matter (SIDM). This result for SIDM is unexpected since in this case the material should be compressed to higher densities during a merger event, sinking to where it reaches the local pressure equilibrium and where the specific entropy matches. Therefore mergers should occur at nearly constant Q rather than constant density.

In a previous investigation (Peirani et al. 2006, hereafter PDP06), we have reported cosmological simulations aiming to study the evolution of the phase-space density indicator Q in core of dark matter halos. Halos were classed in two different catalogs: the *accretion*, comprising 781 objects which have never undergone a major merger event and whose masses varied continuously and smoothly. The *merger catalog* contains 567 halos which had at least one major merger event, corresponding to an increase of their masses at least by a factor 1/3. These simulations indicate that the phase-space density decreases continuously in time, scaling with the velocity dispersion as $Q \propto \sigma^{-2.1}$ and with the halo mass as $Q \propto M^{-0.82}$. No differences in these scaling relations were seen between “cold” and “warm” dark matter models but halos which have underwent important merger events are, on the average, more relaxed having Q values lower than halos of the accretion class. The follow up of individual halos indicates an early and fast phase in which Q decreases on the average by a factor of 40 followed by a long period in which Q further decreases by about factor of 20. The decrease of Q (or the *increase* in the entropy) in the first phase is probably a consequence of the randomization of bulk motions during the first shell crossing while accretion and merger events are responsible for the slow decrease observed in late epochs.

In the present work we report a detailed investigation of 35 CDM halos whose evolution was followed from $z \sim 10$ up to day. For each of these halos, we have estimated the redshift at which the first shell crossing occurs and which we assume to coincide with “virialization”. The phase-space density indicator Q in core of these halos was estimated at that moment and compared with theoretical estimates performed through the spherical model. The agreement between theoretical and numerical estimates confirms our previous conjecture concerning the rapid decrease of Q observed in the early evolutionary phases. We have also studied the late behavior in some specific examples to show the evolution of the velocity distribution during a merger event and the evolution of structures in the phase-space. This paper is organized as follows: in Section 2 we describe briefly the simulations, in Section 3 the phase-space density at “virialization” is discussed, in Section 4 we describe some merger episodes and the behavior of the velocity distribution as well as of structures

in phase-space and, finally, in Section 5 we present our main conclusions.

2. The simulations

In the present work we have used the same halo catalogs as in PDP06, including objects with masses in the range $10^{10} - 10^{13} M_{\odot}$. For the sake of completeness, we summarize here the main steps performed to prepare these catalogs.

The N-body simulation uses the adaptive particle-particle/particle-mesh (AP^3M) code HYDRA (Couchman et al. 1995). The adopted cosmological parameters were $h = 0.65$, $\Omega_m = 0.3$ and $\Omega_{\Lambda} = 0.7$, with the power spectrum normalization $\sigma_8 = 0.9$. The simulation was performed in a box of side $30h^{-1}$ Mpc, including 256^3 particles, corresponding to a mass resolution of $2.05 \times 10^8 M_{\odot}$. The simulation started at $z = 50$ and ended at the present time ($z = 0$). Halos were initially detected by using a friends-of-friends (FOF) algorithm (Davis et al. 1985) and, in a second step, unbound particles were removed by an iterative procedure. Thus, our selected halos are all gravitationally bound objects. In the total, 1348 halos were detected, constituting the two aforementioned catalogs (PDP06). The evolution of these objects was chased from $z = 3.5$ until $z = 0$, but about 40 halos with initially enough particles ($N \geq 50$) were followed during a longer time interval ($10 \leq z \leq 0$). For each halo, we have monitored the evolution of the mass, density, virial ratio and velocity dispersion.

3. The phase-space density at virialization

According to the analysis by PDP06, the phase-space density Q decreases continuously as halos accrete matter. The derivative dQ/dt shows the presence of “valleys” which coincide with peaks in the derivative $d\sigma/dt$ of the velocity dispersion. These structures are always associated with sudden variations in the mass, induced by merger events and leading to a slight “heating”, followed by a relaxation of the system, measured by the decrease in the phase-space density indicator Q , which is equivalent to say that the entropy of the system increased. If this behavior characterizes in general the late evolution of halos, the first and strong peak in the derivative of the velocity dispersion, correlated with the first and deep valley in the derivative of the phase-space density (see Fig. 4 in PDP06), is not a consequence of merging, but probably a consequence of the gravitational collapse. If this interpretation is correct, an important energy transfer from bulk to random motions should occur due to collective effects, heating all the particles, regardless their initial energies.

In order to test our conjecture, we have first derived for a sample of 35 halos, which have been followed in the interval $10 \leq z \leq 0$, which includes the redshift at which the first shell crossing occurs. We assumed here, as in Sugerman et al. (2000), that the first shell crossing episode coincides with the time of maximum velocity dispersion as well as with “virialization”. In fact, as halos accrete mass, the virial ratio $2T/|W|$ approaches asymptotically the unity and, just after the first shell crossing, they are only in quasi dynamical equilibrium. For our subsequent analysis, we assume for simplicity that the relaxation process was almost achieved.

In fig. 1, the halo mass is plotted as a function of the redshift z_v at which “virialization” occurs. Notice that, as expected in the hierarchical picture, less massive halos collapse first and that

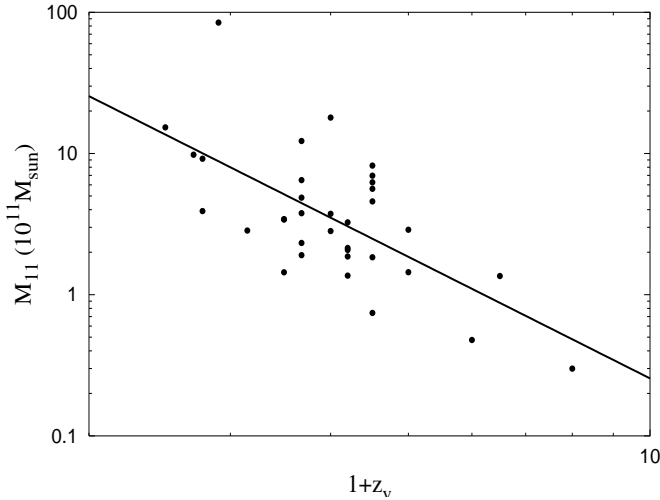


Fig. 1. The halo mass as a function of the redshift z_v at which “virialization” occurs (defined as the time of maximum velocity dispersion). The solid line represents the best fit solution.

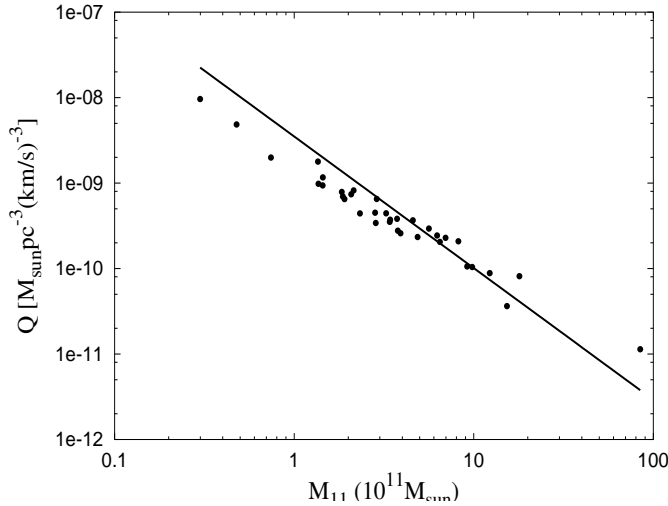


Fig. 2. The phase-space density Q as a function of the halo mass. The points represent values derived from simulated data whereas the solid line is obtained from relation (8).

large galaxy-size halos ($\sim 10^{12} M_\odot$) are being virialized around $z_v \sim 1 - 2$. A best fit of these simulated data gives

$$M_{11} = \frac{185}{(1 + z_v)^{2.86}} \quad (1)$$

where M_{11} stands for the halo mass in units of $10^{11} M_\odot$.

The phase-space density Q at “virialization” was calculated as follows: for each halo, the gravitational radius $r_g = GM/|W|$ was computed as well as the mean density $\bar{\rho} = 3M/(4\pi r_g^3)$. The 1-D velocity dispersion σ was calculated by assuming isotropy, e.g., $\sigma = \sqrt{(\sigma_x^2 + \sigma_y^2 + \sigma_z^2)/3}$ and, finally the phase-space density indicator, $Q = \bar{\rho}/\sigma^3$.

In order to perform a theoretical estimate of the value of the phase-space density Q just after virialization, we have appealed to the spherical collapse model, including effects of a cosmological constant, in order to be consistent with the cosmology adopted in our simulations.

The expected density contrast at virialization, using the results of Bryan & Norman (1998), is approximately given by

$$\Delta_v = 18\pi^2 + 82[\Omega_m(z_v) - 1] - 39[\Omega_m(z_v) - 1]^2 \quad (2)$$

Thus, the mean halo density at virialization is

$$\rho_v = \Delta_v \frac{3H_0^2}{8\pi G} \Omega_m^0 (1 + z_v)^3 = \frac{3M}{4\pi R_v^3} \quad (3)$$

where Ω_m^0 is the present matter (dark+baryonic) density parameter and R_v is the radius at virial equilibrium.

Defining the ratio between the virialization and the turnaround radii as $\eta = R_v/R_0$ and using the energy conservation as well as the virial relation, one obtains (Lahav et al. 1991)

$$\lambda\eta^3 - 2(2 + \lambda)\eta + 2 = 0 \quad (4)$$

where we have introduced the parameter $\lambda = \Omega_v H_0^2 R_0^3 / GM$. The solution of this cubic equation can approximately be expressed by

$$\eta = 0.5 - 0.20936\lambda + 0.04949\lambda^2 \quad (5)$$

Since the ratio between densities at turnaround and virialization is $\rho_{ta}/\rho_v = \eta^3$, using eq.(3) and the definition of the parameter λ one obtains

$$\lambda\eta^3 = \frac{3\Omega_v H_0^2}{4\pi G \rho_v} \quad (6)$$

On the other hand, since $3\sigma^2 = -2E$, where E is the total energy, we can express the 1-D velocity dispersion as

$$\sigma^3 = \left[\frac{2}{3\lambda^{1/3}} + \frac{\lambda^{2/3}}{3} \right]^{3/2} (\Omega_v H_0^2)^{1/2} GM \quad (7)$$

Therefore, the procedure adopted to estimate Q was: for a given virialization redshift z_v , one computes the virialization density ρ_v from eqs. (2) and (3). Then, using eqs. (5) and (6) the value of λ at the considered z_v is derived. This value is used in eq. (7), together with the mass M virializing at z_v and estimated from eq. (1), to obtain the velocity dispersion. The resulting values of the phase-space density Q are quite well fitted by the relation

$$Q \approx \frac{3.51 \times 10^{-9}}{M_{11}^{1.54}} M_\odot \text{pc}^{-3} \text{km}^{-3} \text{s}^{-3} \quad (8)$$

Figure 2 compares the expected values of the phase-space density Q as a function of the halo mass, computed from the equation above and values derived from simulated data. The agreement is quite good in spite of the fact that the model assumes a constant halo mass, but confirms our previous conjecture that the early and fast decrease of the phase-space density observed in the halo history reflects the “thermalization” of bulk motions.

4. Phase-Space Mixing in Mergers

In the late evolutionary phases of dark matter halos, the rate at which the phase-space density decreases depends on the frequency of mergers and on the amount of mass accreted in these events. Subhalos captured in quite eccentric orbits are generally disrupted completely by tidal forces, transferring angular momentum to the host halo and thus increasing its spin (Peirani et al. 2004) but forming, as we shall see latter, streams detectable in

phase-space diagrams before to mix completely with the background material.

An attempt to verify whether the merging history of our Galaxy left “finger-prints” in the phase-space structure of nearby stars was made by Helmi & White (1999). In that investigation, the infall of satellites onto a fixed potential was followed numerically as well as the evolution of the debris in phase-space. Helmi & White found that after ~ 10 Gyr, stars having a common origin are distributed smoothly in space, but form clumps in velocity space.

We have searched in our simulation for merger episodes involving massive halos, e.g., having a mass greater than $10^{12} M_{\odot}$ at $z = 0$, in order to perform evolutionary studies in the phase-space.

The first example consists of a main halo having presently a mass of about $4.0 \times 10^{12} M_{\odot}$, which was caught in the act of capture of two subhalos (at $z = 0.92$) with masses at that moment respectively equal to $1.6 \times 10^{11} M_{\odot}$ (subhalo-1) and $2.8 \times 10^{11} M_{\odot}$ (subhalo-2). The orbits of each subhalo are sketched in fig. 3. The trajectory of the center of mass of subhalo-1 is represented both in the orbital and in the transversal planes in the first two panels. The trajectory of subhalo-2 is represented in the orbital plane up to $z = 0.48$ only, since its identity is completely lost at late times. Subhalo-1 has an impact parameter or orbital angular momentum higher than the subhalo-2, illustrating the well known effect of this dynamical parameter on the tidal stripping of captured objects.

Successive snapshots of the phase-space evolution (radial velocity versus radial distance) are shown in fig. 4. The subhalo-1 has an orbital period of about 6 Gyr and its periastron is about 100 kpc. Tidal forces strip off only the outer and loosely bound particles, the object preserving most of its identity after 8 Gyr. However, already at $z \approx 0.67$ (near periastron), stripped particles with high positive velocities can be seen, while the bulk has negative values. Effects in the velocity distribution are better visualized in fig. 5, where the corresponding radial velocity distributions are shown for each snapshot of fig. 4. Initially ($z = 0.92$) three distinct velocity distributions can be identified, associated respectively to the main halo and the two subhalos, with velocity dispersions of $\sigma_H = 202$ km/s, $\sigma_1 = 51$ km/s and $\sigma_2 = 78$ km/s. For comparison, the best fitted Gaussians are also shown as solid lines. In spite of subhalo-1 to have preserved its identity, stripped particles mix in the velocity space and this process can be followed in the different snapshots either in fig. 4 or fig. 5. Notice in particular the appearance of extended tails in the velocity distribution of the captured halos. Subhalo-2 has a short orbital period (~ 2 Gyr) and a quite eccentric orbit. Extended tidal arms are developed after the various periastron passage, forming structures spatially displaced by the orbital decay resulting from dynamical friction. In this case, the mixing in the velocity space (see, fig. 5) is quite efficient and after 3.4 Gyr the particle velocity distribution of subhalo-2 coincides practically with that of the main halo.

In spite of Gaussians be able to fit reasonable well the radial velocity distribution of the main halo (mean determination coefficient $r = 0.97$) and satellites (but $r = 0.86$ for subhalo-2), we have also calculated the kurtosis, $k = (\langle v^4 \rangle / \langle v^2 \rangle^2) - 3$, for both the main halo and the subhalo-2 at $z = 0$. For the main halo, the kurtosis was evaluated for ten shells with 2800 particles each, while for subhalo-2 we have considered only three shells with about 400 particles each. No particular trend with the radial distance was found, with the main halo having a mean kurtosis $k = -0.57$ and the subhalo-2 $k = -0.73$. These values indicate that the radial velocity distribution is flat-topped with respect to

a Gaussian and that the effect is more accentuated in the resulting substructure.

Another interesting case of capture is illustrated by our second example. Here the main halo has a mass of about $3.3 \times 10^{12} M_{\odot}$ and the capture of a satellite with a mass of $5.2 \times 10^{11} M_{\odot}$ occurs at $z = 0.92$. Here again masses correspond to that instant, since at the end, due to the continuous infall process, masses are substantially higher. Fig. 6 shows snapshots of the phase space at different redshifts. Structures are gradually formed as the satellite passes by periastron. The observed streams in the phase-space are very similar to those derived from models of halo formation by secondary infall (see, for instance, Sikivie et al. 1997 and references therein). However, structures seen in the latter case are formed by successive passages of infalling (or outgoing) particles and are associated to “caustics”. From a mathematical point of view, caustics have an infinite density. In physical systems, the density is limited by the fact that the motion of DM particles is not purely radial (non-zero angular momentum) and by a non-zero velocity dispersion (Sikivie et al. 1997). If the nature of DM particles is specified, then other constraints can be imposed. For instance, neutralinos and anti-neutralinos may annihilate with a rate proportional to the square of their density, a mechanism which imposes upper bounds to the density. Moreover, neutralinos are fermions and one would expect that a “classical” behavior must be abandoned when their de Broglie wavelength will be greater than the mean inter-particle separation. This occurs for densities n satisfying $n > (m_{\chi} v / h)^3$, when repulsive forces of quantum nature due to the Pauli principle become effective, introducing a further physical mechanism able to impose limits on the density. In a given instant and for a fixed value of the radial distance, a certain number of velocity peaks, corresponding to different streams can be seen in the phase-space diagram (Fig. 6), which depends on the initial angular momentum, as simulations suggest. In the extreme limit of circular orbits only one stream should be observed, a case comparable to that of satellite-1 in the first example. The width δv_m of the m-velocity peak associated to the m-caustic is generally estimated from the Liouville theorem, using the velocity dispersion and density at the moment of their first turnaround. In general and in the present case, this procedure can not be applied. The fine-grained DF is strictly conserved in the phase-space flow but this is not the case of the coarse-grained DF, since phase-space elements of high density are stretched out and folded with elements of low density because of mixing (Lyndell-Bell 1967).

It’s worth mentioning that the time evolution of the virial ratio $2T/|W|$ of the whole system has clear maxima corresponding to successive pericenter passages of the center of mass of the sub-halo (see Fig. 7), in agreement with merger simulation by Valluri et al. (2007). However, in this particular case, there is no expressive redistribution of the specific angular momentum \mathbf{j} after the merger event, the radial profiles of \mathbf{j} being practically the same before and after merging (see fig. 8), since the collision orbit is almost radial and, consequently, no significant transfer of angular momentum occurs. As in the previous example, the analysis of the kurtosis at $z = 0$ indicates top-flatted velocity distributions with the satellite-1 having a flatter distribution (mean kurtosis $k = -0.85$ in comparison with $k = -0.64$ for the main halo).

In the third example of a merger episode, the main halo has a mass of $4.3 \times 10^{12} M_{\odot}$ and underwent an important fusion at $z=0.92$, since the captured object has a comparable mass ($\sim 1.2 \times 10^{12} M_{\odot}$). In the three upper panels of fig. 9, the phase-space evolution is shown at three distinct redshifts. At $z = 0.48$, structures formed at different periastron passages can be seen,

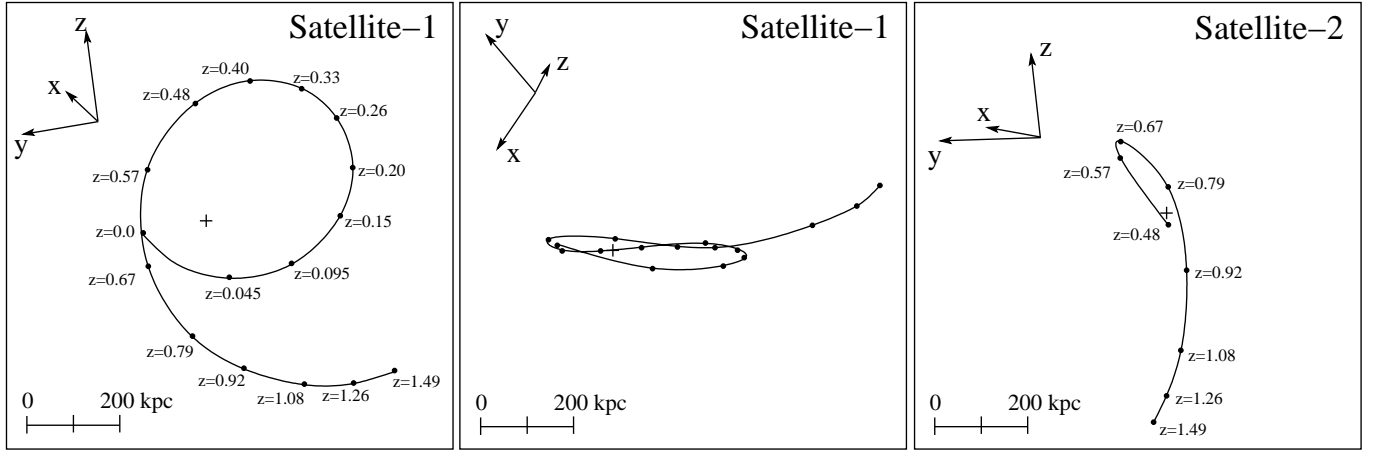


Fig. 3. Sketch of the orbits of satellites in 3D-space for example 1. In the left and right panels, the motion in the orbital plane is represented for both satellites, while in the middle panel the motion of satellite-1 is represented in the transversal plane. The cross indicates the position of the center of mass of the system.

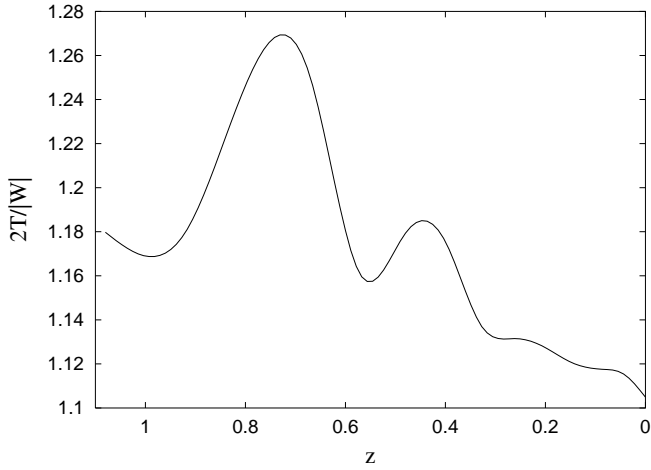


Fig. 7. The evolution of the virial ratio $2T/|W|$ as a function of the redshift (example 2). Each maximum corresponds to the passage of the subhalo by periastron.

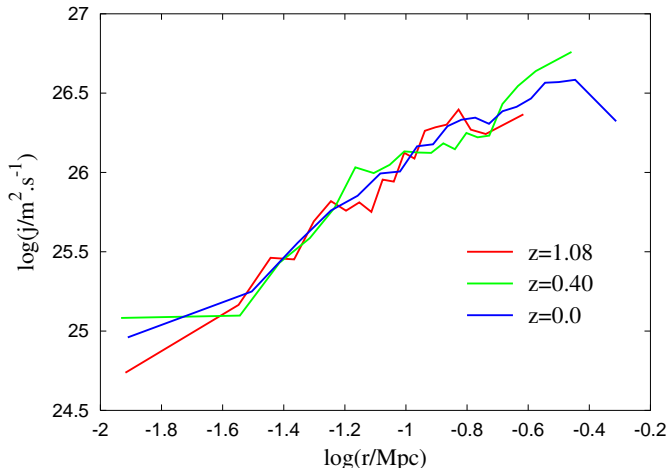


Fig. 8. The radial profile of the specific angular momentum j for the merger example 2. Consequence of a "head-on" collision, no significant modifications in the profile of j is observed after the merger event ($z = 0$) which occurred at $z = 1.08$.

while at $z = 0$ the captured halo is completely disrupted and its particles are well mixed in phase-space. This behavior is consistent with the simulations by Valluri et al. (2007), which indicate that mixing in the space of the dynamical variables (E, J) occurs primarily during periastron passages and are driven probably by compressive tidal shocks. The subsequent panels show the evolution of the radial velocity distribution. The second line shows the evolution for all particles of the main halo and satellite, which at $z = 0.92$ has a velocity dispersion of 130 km/s. At $z = 0.48$ and $z = 0$ both velocity distributions practically match. The average kurtosis are $k = -0.57$ and $k = -0.65$ for the main halo and satellite respectively, confirming the trend that substructures have top-flatted velocity distributions more accentuated than those of the main halos.

Notice that the fact that all selected merger examples occur at $z = 0.92$ is completely fortuitous and is probably associated to a maximum rate of mergers around $z \sim 1$ as well as to the time resolution adopted in the present study.

The main halos in the aforementioned examples have typically $(3 - 4) \times 10^4$ particles while for satellites the numbers are about one order of magnitude lower. In the simulations by Wojtak et al. (2005), cluster size halos with few times 10^4 particles (numbers comparable to those of our selected examples) were considered. These authors concluded that the velocity distribution of main halos are only Gaussian to a good approximation near the center, but more and more flat-topped with respect to Gaussians when approaching the virial radius. Numerical experiments of higher resolution were performed by Diemand et al. (2004) and Kazantzidis et al. (2004). The former authors considered galactic and cluster size halos extracted from cosmological simulations, including several millions of particles. They concluded that subhalos have flat-topped velocity distributions with a typical kurtosis $k \simeq -0.7$. Equilibrium halos with about 10^5 particles were generated by Kazantzidis et al. (2004) using the Eddington method. They found also that the velocity distribution of such systems are less peaked than Gaussians.

In spite of the different employed resolutions, all these investigations (including our own) lead to consistent results, e.g., the velocity distribution of halos are flat-topped with kurtosis in the range $-0.4 > k > -0.9$.

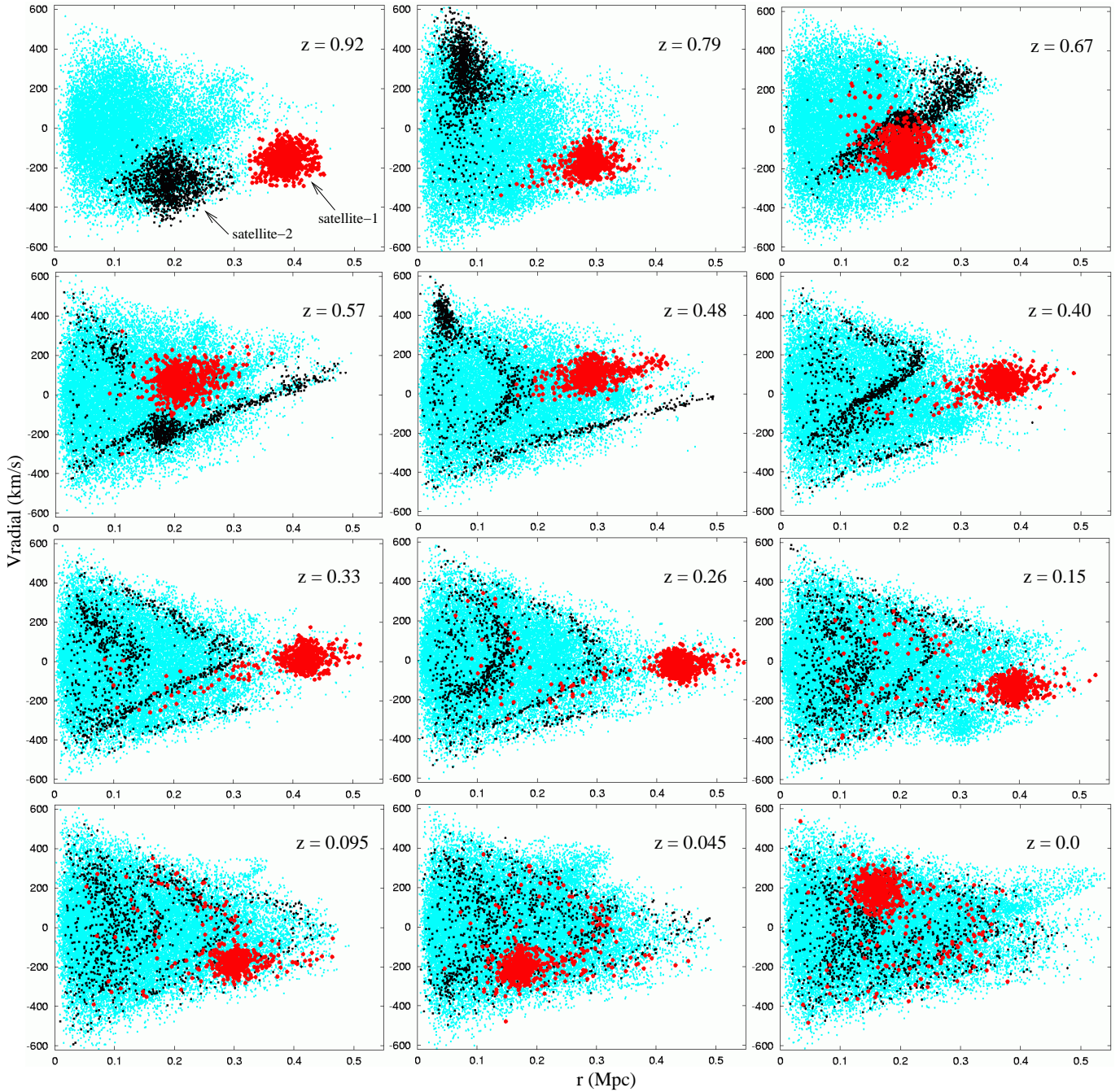


Fig. 4. The phase-space evolution (radial velocity versus radial distance) for the host halo and satellites of example 1. Upper right labels indicate the redshift. Satellite-1 and Satellite-2 are respectively represented by red and black points.

5. Conclusions

The dynamical evolution of dark matter halos after the gravitational collapse depends on their accretion history. The phase-space density indicator Q decreases by a large factor (~ 40) during the first shell crossing as a consequence of the randomization process of initial bulk motions. Our theoretical estimates of the phase-space density Q based on the spherical collapse model are in agreement with our simulated data, suggesting that at “virialization” the phase-space density scales with the halo mass as $Q \propto M^{-1.5}$. The analysis by Armarzguioui & Gron (2005) indicates that the entropy of an ideal gas increases to the first order in the gravitational collapse within the context of the FRW cosmology. This entropy increase is a consequence of the transfer of

gravitational potential energy to thermal energy during the collapse, a process similar to that observed for collisionless matter. Effects of shell crossing play probably a non negligible role in the way halos reach equilibrium and should be taken into account in future studies, since they affect the resulting “virial” radius of the system (Sánchez-Conde et al. 2006).

Non-disrupted satellites develop high velocity tails in their radial velocity distribution. The mechanism (or mechanisms) responsible for such a heating is not well established. Funato, Makino & Ebisuzaki (1992) based on N-body simulations of collisionless systems argued that wave-particle interactions, e.g., collective effects driven by large fluctuations of the gravitational potential are able to produce a substantial heating in a few dynamical time scales, regardless the particle initial en-

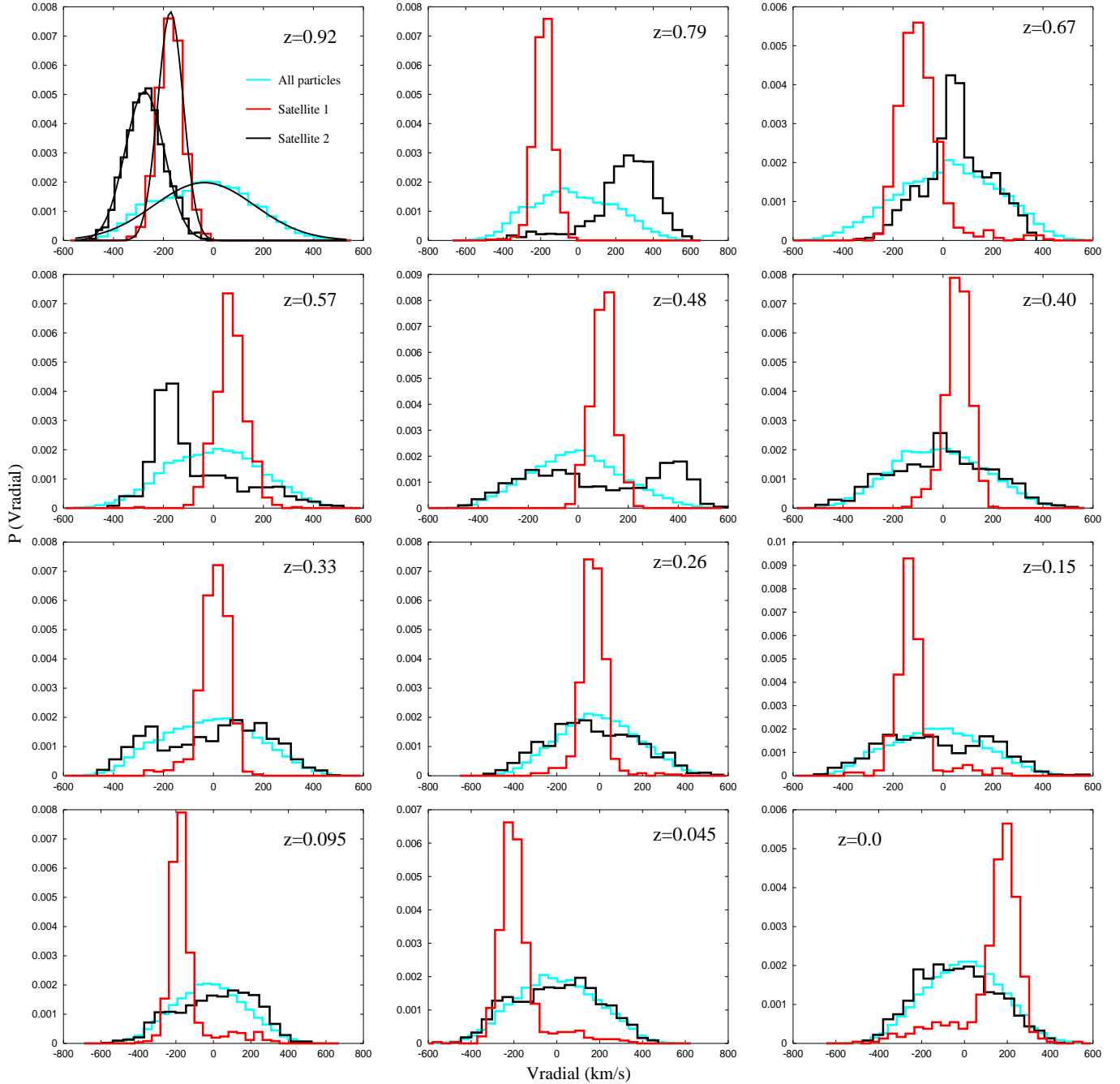


Fig. 5. The evolution of the radial velocity distribution for the host halo (light blue), satellite-1 (red) and satellite-2 (black) for example 1. At $z = 0.92$, the best fitted Gaussian distribution is superimposed to histograms. Notice that the velocity distribution of satellite-1 is preserved but it develops high velocity tails.

ergy. Another possibility is the heating produced by compressive tides that arise when one collisionless gravitating system passes through another on a time scale shorter than the internal dynamical time of the infalling object. Such tides can impulsively heat particles as a result of the transient deepening of the net gravitational potential (Valluri et al. 2007). Impulsive compressive tidal shocks are well known to produce changes in the internal structure of globular clusters (Gnedin et al. 1999) or in subhalos orbiting within massive hosts (Kravtsov et al. 2004).

Disrupted satellites leave “finger-prints” in phase-space, generating streams which depend on the initial orbital angular momentum and which remind caustic structures seen in sec-

ondary infall models of halo formation. Future high resolution simulations will certainly give a better insight on the evolution of these structures. It is worth mentioning that extended secondary infall models are also able to explain the scaling-free Q profile (Austin et al. 2005). Stars behave as a collisionless fluid similar to dark matter. In this case, one should expect that disrupted satellites will form not only dark matter streams but also stellar streams, which could eventually be detected in phase-space by the forthcoming space mission GAIA as also suggested by Brown et al. (2005).

Our previous study (PDP06) and the present work support the view that violent variations in the gravitational potential,

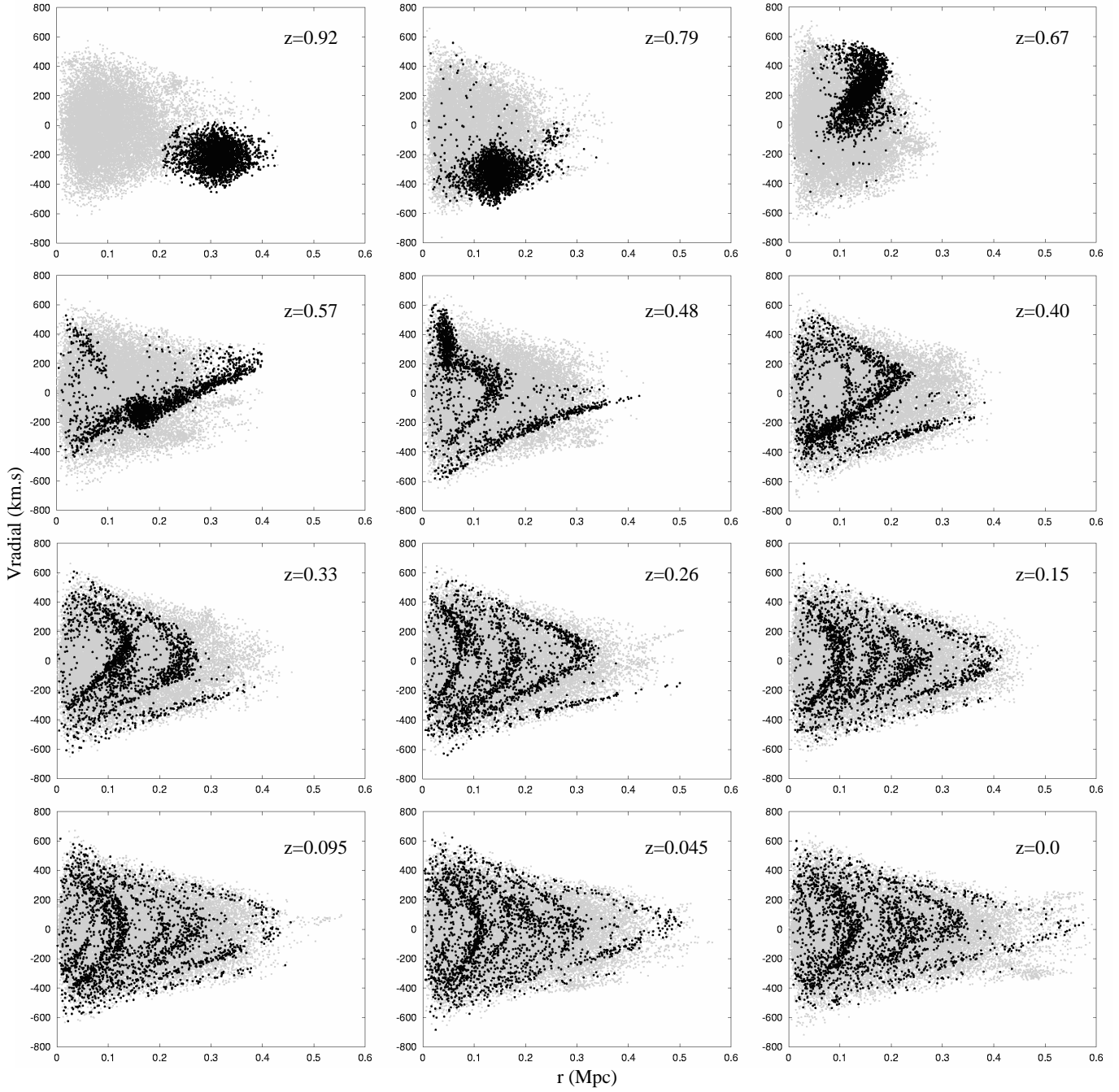


Fig. 6. The phase-space evolution of the host halo and satellite (black points) for example 2. The latter is completely disrupted by tidal forces. The different snapshots show the formation of streams in phase-space.

which occur in important merger events, lead to more mixed systems as the temporal behaviour of the phase-space density suggests. The study of some merger episodes indicates that the radial velocity of completely disrupted satellites and that of the main halo fuse in a common distribution in a few dynamical time scales. Quasi-relaxed halos have top-flatted velocity distributions, which are observed not only for the bulk of particles but also for particles inside shells at different distances from the center. The significance of these top-flatted profiles is measured by the kurtosis (always negative) and this effect is more accentuated for captured subhalos and/or substructures in comparison with the velocity distribution of the main halo. Kazantzidis et al. (2004) have developed an algorithm for constructing N-

body realizations of equilibrium spherical systems, which differs from the usual assumption that the local velocity distribution is Maxwellian. Equilibrium halo models built through their procedure when evolved, develop velocity distributions less peaked than Gaussians and the disruption time scale of captured satellites becomes significantly longer in comparison with initial Maxwellian equilibrium models. Cosmological simulations by Diemand et al. (2004) lead also to the conclusion that substructures of either galactic-size or cluster-size halos have top-flatted velocity profiles, in agreement with our results. Moreover, an investigation of structures resulting from head-on collisions of halos having a Navarro-Frenk-White density profile was performed by Hansen et al. (2006). They concluded that the phase-space

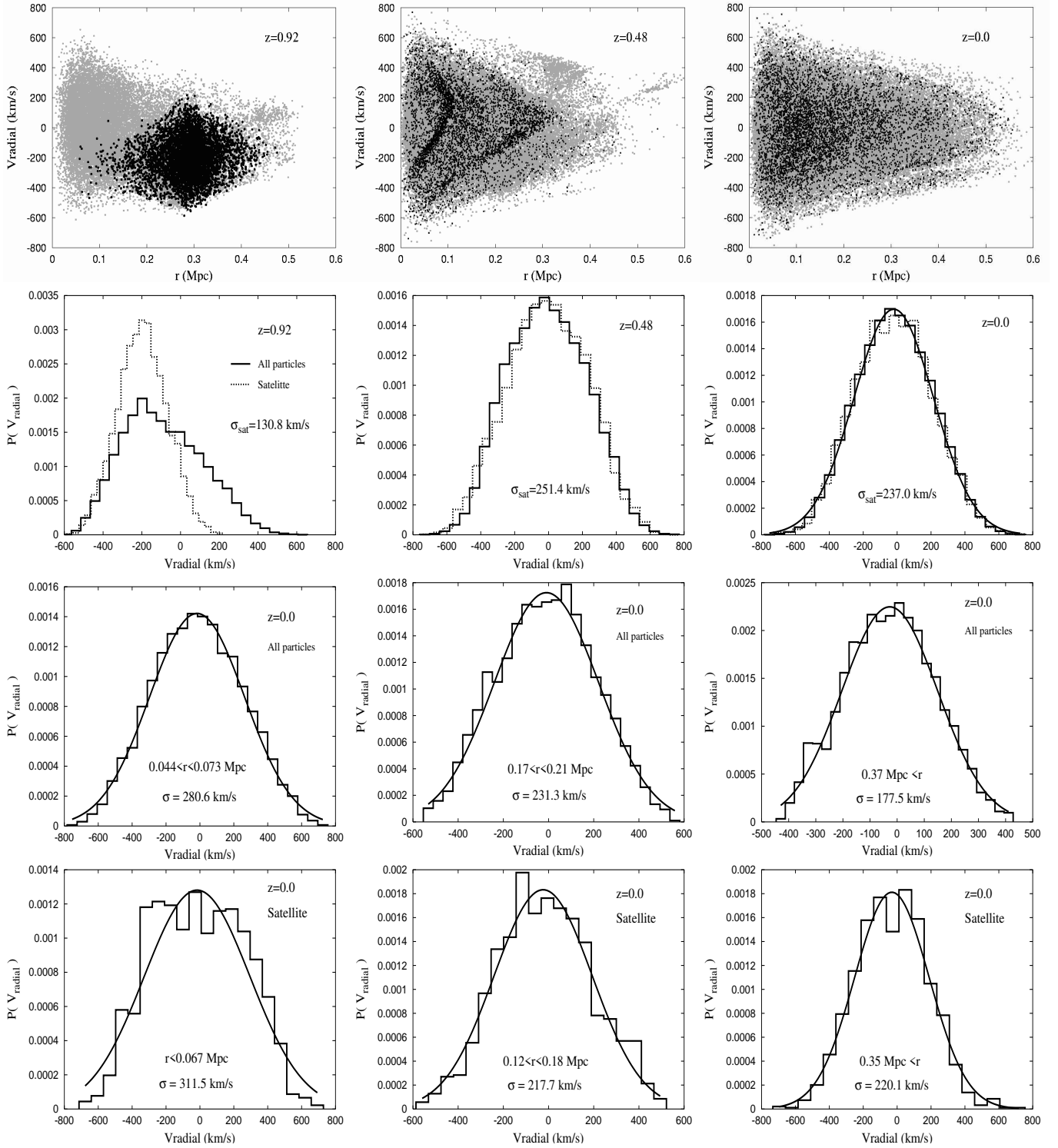


Fig. 9. (Top) The phase-space evolution of the main halo and a satellite (black points) completely disrupted by tidal forces, in example 3. The other panels show respectively the evolution of the radial velocity distribution for all particles of both host and satellite (second line), and the radial velocity distribution at different shells from the center (all particles, third line and for the satellite, fourth line). Solid lines represent the best Gaussian fit.

density indicator Q has a power-law distribution and that the resulting velocity distribution is not Gaussian, but can be represented by a function derived from the Tsallis statistics (Tsallis 1988). Thus, deviations from Gaussianity seems to be a quite general result and, in this sense, the present simulations repre-

sent a contribution to establish an empirical basis for future theoretical developments in this area.

Acknowledgements. S.P. acknowledges the financial support from a ANR grant. S.P. is grateful to R. Mohayaee for discussions on the early phase of this work. We also thank S. Hansen and F. Durier for their useful comments which have significantly improved this paper.

References

- Arad, I., Dekel, A. and Klypin, A., 2004, MNRAS 353, 15
- Armarzguoui, M. and Gron, O., 2005, PRD 71, 083011
- Ascasibar, Y., Yepes, G., Gottlöber, S., Müller, V. 2004, MNRAS, 352, 1109
- Ascasibar, Y., & Gottlöber, S. 2008, MNRAS, 386, 2022
- Austin, C.G., Williams, L.L.R., Barnes, E.I., Babul, A. and Dalcanton, J.J., 2005, ApJ 634, 756
- Boylan-Kolchin, M., & Ma, C.-P. 2004, MNRAS, 349, 1117
- Bryan, G.L. and Norman, M.L., 1998, ApJ 495, 80
- Brown, A. G. A., Velázquez, H. M., & Aguilar, L. A. 2005, MNRAS, 359, 1287
- Couchman, H.M.P., Thomas, P.A. and Pearce, F.R., 1995, ApJ 452, 797
- Dalcanton, J.J. and Hogan, C.J., 2001, ApJ 561, 35
- Davé, R., Spergel, D.N., Steinhardt, P.J. and Wandelt, D., 2001, ApJ 547, 574
- Davis, M., Efstathiou, G., Frenk, C. S., and White, S. D. M. 1985, ApJ, 292, 371
- Dehnen, W., 2005, MNRAS 360, 892
- Dehnen, W., & McLaughlin, D. E. 2005, MNRAS, 363, 1057
- Diemand, J., Moore, B. and Stadel, J., 2004, MNRAS 352, 535
- Funato, Y., Makino, J. and Ebisuzaki, T., 1992, PASJ 44, 613
- Gnedin, O.Y., Lee, H.M. and Ostriker, J.P. 1999, ApJ 522, 935
- Hansen, S.H., Moore, B., Zemp, M. and Stadel, J., 2006, JCAP 0601, 014
- Helmi, A. and White, S.D.M., 1999, MNRAS 307, 495
- Hoffman, Y., Romano-Díaz, E., Shlosman, I., & Heller, C. 2007, ApJ, 671, 1108
- Kazantzidis, S., Magorrian, J. and Moore, B., 2004, ApJ 601, 37
- Knollmann, S. R., Knebe, A., & Hoffman, Y. 2008, MNRAS, 391, 559
- Kravtsov, A.V., Gnedin, O.Y. and Klypin, A.A., 2004, ApJ 609, 482
- Lahav, O., Lilje, P.B., Primack, J.R. and Rees, M.J., 1991, MNRAS 251, 128
- Lynden-Bell, D., 1967, MNRAS 136, 101
- Peirani, S., Mohayaee, R. and de Freitas Pacheco, J.A., 2004, MNRAS 348, 921
- Peirani, S., Durier, F. and de Freitas Pacheco, J.A., 2006, MNRAS 367, 1011 (PDP06)
- Rasia, E., Tormen, G. and Moscardini, L., 2004, MNRAS, 351, 237
- Sánchez-Conde, M. A., Betancort-Rijo, J., & Prada, F. 2007, MNRAS, 378, 339
- Sikivie, P., Tkachev, I.I. and Wang, Y., 1997, Phys.Rev. D56, 1863
- Sugerman, B., Summers, F.J. and Kamionkowski, M., 2000, MNRAS 311, 762
- Taylor, J.E. and Navarro, J.F., 2001, ApJ 563, 483
- Tremaine, S., Hénon, M. and Lynden-Bell, D., 1986, MNRAS 219, 285
- Tsallis, C., 1988, J.Stat.Phys. 52, 479
- Valluri, M., Vass, I.M., Kazantzidis, S., Kravtsov, A.V. and Bohn, C.L., 2007, ApJ 658, 731
- Vass, I. M., Valluri, M., Kravtsov, A., & Kazantzidis, S. 2008a, arXiv:0810.0277
- Vass, I. M., Kazantzidis, S., Valluri, M., & Kravtsov, A. V. 2008b, arXiv:0812.3659
- Wechsler, R.H., Bullock, J.S., Primack, J.R., Kravtsov, A.V. and Dekel, A., 2002, ApJ, 568, 52
- Wojtak, R., Lokas, E.L., Gottloeber, S. and Mamon, G., 2005, MNRAS